Confinement of two-body systems and calculations in d dimensions

E. Garrido[1] and A. S. Jensen[2]
[1]*Instituto de Estructura de la Materia, IEM-CSIC, Serrano 123, E-28006 Madrid, Spain*
[2]*Department of Physics and Astronomy, Aarhus University, DK-8000 Aarhus C, Denmark*

(Received 20 June 2019; published 6 September 2019)

A continuous transition for a system moving in a three-dimensional (3D) space to moving in a lower-dimensional space, 2D or 1D, can be made by means of an external squeezing potential. A squeeze along one direction gives rise to a 3D to 2D transition, whereas a simultaneous squeeze along two directions produces a 3D to 1D transition, without going through an intermediate 2D configuration. In the same way, for a system moving in a 2D space, a squeezing potential along one direction produces a 2D to 1D transition. In this work we investigate the equivalence between this kind of confinement procedure and calculations without an external field, but where the dimension d is taken as a parameter that changes continuously from $d = 3$ to $d = 1$. The practical case of an external harmonic oscillator squeezing potential acting on a two-body system is investigated in detail. For the three transitions considered, 3D $\rightarrow$ 2D, 2D $\rightarrow$ 1D, and 3D $\rightarrow$ 1D, a universal connection between the harmonic oscillator parameter and the dimension d is found. This relation is well established for infinitely large 3D scattering lengths of the two-body potential for 3D $\rightarrow$ 2D and 3D $\rightarrow$ 1D transitions, and for infinitely large 2D scattering length for the 2D $\rightarrow$ 1D case. For finite scattering lengths size corrections must be applied. The traditional wave functions for external squeezing potentials are shown to be uniquely related to the wave functions for specific noninteger dimension parameters, d.

DOI: 10.1103/PhysRevResearch.1.023009

I. INTRODUCTION

The properties of quantum systems depend crucially on the dimension of the space where they are allowed to move. A clear example of this is the centrifugal barrier in the radial Schrödinger equation, which, for zero total angular momentum, is negative for a two-body system in two (2D) dimensions, while it is zero in three (3D) dimensions [1]. An immediate consequence of this is that any infinitesimal amount of attraction produces a bound state in 2D, whereas in 3D a finite amount of attraction is necessary for binding a system [2]. As an exotic example of recent interest we can mention, at the three-body level, the occurrence in 3D of the Efimov effect [3]. In 2D, this effect does not occur, neither for equal-mass three-body systems [4] nor for unequal-mass systems [5].

The transition from a three-dimensional to a lower-dimensional space is commonly investigated by means of an external trap potential that confines the system under investigation in a certain region in the space. In this way, in [6] a harmonic oscillator trap potential is used, and binary atomic collisions are investigated under different confinement regimes. This work focus on scattering properties in confined spaces, not necessarily similar to the asymmetric squeezing of only one or two spatial dimensions. More recently, the particle-physics formalism has been specifically extended to connect $d = 3$ and $d = 2$ by continuously compactifying, by means of an infinite potential well, one of the dimensions [7–9]. Working in momentum space, the intentions were to study three-body physics, but two-body subsystems are then necessary ingredients. The physical interpretation of the squeezing parameter in this procedure is a problem necessary to be addressed to connect properly to measurements. The same compactifying procedure along one or two directions has been employed to investigate the S matrix for two-body scattering [10], and again the focus is on scattering under confining conditions. Another structure-related investigation has appeared in the literature, that is, the superfluid phase transition temperature in the crossover from three to two dimensions [11]. This is necessarily a many-body effect although prompted by two-body properties.

In all these works the procedure has been to perform genuine 3D calculations where the external potential enters explicitly in order to limit the space available. However, an alternative can be to employ an abstract formulation where the dimension d can take different values describing the different possible scenarios. For instance, in [12] an expansion in terms of $1/d$ is performed, where d is thought of as an integer, allowing extrapolations between integers. The philosophy has been to extrapolate obtainable results as function of $1/d$ for very large d and first down to $d = 3$ for two or more particles [13]. Going further down toward $d = 2$ is probably going too far [13], both because $1/d = 1/2$ is not very large, but especially because the properties change qualitatively from $d = 3$ to $d = 2$. Noninteger dimensions have also been employed in various subfields of mathematics and physics; see, e.g., [14,15]. For many particles even mixed dimensions have been

used to study exotic structures [9]. A practical continuous connection between integer dimensions is interesting in order to understand the related structure variations.

In this work the approach would be formulation in coordinate space by simple analytic continuation of the abstract formulation in terms of the dimension parameter d assuming noninteger values. The limits of $d = 1, 2, 3$ are now well defined in contrast to any value between these integers. A practical interpretation can be found by use of deformed external fields squeezing one or more dimensions to zero spatial extension corresponding to infinitely high zero-point energy. This method was used in a recent work [16], where the continuous confinement of quantum systems from three to two dimensions was investigated.

The confinement in [16] was treated by use of two different procedures. In the first one the particles are put under the effect of an external trap potential acting on a single direction. This potential continuously limits the motion of the particles along that direction, in such a way that for infinite squeezing the system moves in a 2D space. In the second method the external potential is not used, and the problem instead is solved directly in d dimensions, where d is a parameter that changes continuously from 3 to 2. This formulation has the advantage that the numerical effort required is similar to solving the ordinary problem for integer dimensions.

In [16] the 3D to 2D confinement was investigated for two-body systems and external harmonic oscillator confining potentials. The purpose of this work is to extend the investigation to squeezing up to one dimension (1D). This can be done in two different ways. In the first one we consider a simultaneous squeezing along two directions, in such a way that the external potential pushes the system, initially moving in 3D, to moving in 1D without going through an intermediate 2D geometry. The second procedure consists of two consecutive squeezing processes along one direction, giving rise to a 3D to 2D squeezing followed by a 2D to 1D squeezing. The obvious, but complicated, extension to systems made of more than two particles is left for a forthcoming work.

In all the confinement scenarios (3D $\rightarrow$ 2D, 2D $\rightarrow$ 1D, and 3D $\rightarrow$ 1D) the problem will be treated by means of the two procedures described above, i.e., by explicit use of the confinement potential, and by use of the dimension d as a parameter that changes continuously from $d = 3$ to $d = 2$ or $d = 1$. One of the main goals is then, for all the cases, to establish the equivalence between a given value of the confining harmonic oscillator frequency and the dimension d describing the same physical situation.

The connection between the harmonic oscillator parameter and the dimension d should preferentially be universal in the sense of being independent of the details of the potential. It is well known that necessary ingredients for the appearance of universal properties of quantum systems are the existence of two-body interactions with large scattering lengths, and, to a large extent, the preponderance of relative s waves between the constituents. The existence, under these conditions, of a universal connection between the harmonic oscillator parameter and the dimension will be investigated. Here it is clear that large squeezing confining a wave function to be inside the two-body potential must depend on potential details. However, comparing the two methods, it can still result in the same universal dependence, since both are subject to the same potential. To be practical, we have established such a highly desirable connection between the wave functions obtained in the two methods.

The overall purpose of the present work is therefore to study a number of different transitions between integer dimensions, and to establish the universal connection between the d-parameter results and those of the brute-force three-dimensional calculation with a deformed external field. The connection must allow the numerically simpler d method to be self-sufficient, that is, in itself providing full information including correspondence to an external field and three-dimensional wave function. The paper is organized as follows. In Sec. II we describe the procedure used to confine a two-body system by use of an external harmonic oscillator potential. In Sec. III we briefly describe the method used to solve the two-body problem in d dimensions. Section IV presents analytic results in the large squeezing limit, that is, close to one or two dimensions. Sections V and VI present and discuss the numerical results, and Sec. VII gives the universal translation between the two methods. Finally, Sec. VIII contains a summary, and the future perspectives are briefly discussed. A mathematical connection between wave functions from the two methods is given in the Appendix.

II. HARMONIC OSCILLATOR SQUEEZING

A simple way to confine particles is to put them under the effect of an external potential with steep walls that forces them to move in a confined space. Therefore, the problem to be solved is the usual Schrödinger equation, but where, together with the interaction between the particles, the confining one-body potential has to be included.

In this work we shall consider an external harmonic oscillator potential whose frequency will be written as

$$\omega = \frac{\hbar}{m_\omega b_{\rm ho}^2}, \tag{1}$$

where m_ω is some arbitrary mass. Obviously, the smaller the harmonic oscillator length $b_{\rm ho}$, the more confined the particles are in the corresponding direction.

In the following we describe how this harmonic oscillator potential is treated for the three confinement cases, 3D $\rightarrow$ 2D, 2D $\rightarrow$ 1D, and 3D $\rightarrow$ 1D, considered in this work.

A. 3D $\rightarrow$ 2D

In this case the external harmonic oscillator potential is assumed to act along the z direction. Therefore, the problem to be solved here will be the usual three-dimensional two-body problem but where, on top of the two-body interaction, each of the two particles feels the effect of the external trap potential:

$$V_{\rm trap}^{(i)} = \frac{1}{2} m_i \omega^2 r_i^2 \cos^2\theta_i = \frac{1}{2} \frac{m_i \hbar^2}{m_\omega^2 b_{\rm ho}^4} r_i^2 \cos^2\theta_i, \tag{2}$$

where Eq. (1) has been used, and where r_i and θ_i are the radial coordinate and polar angle associated with particle i with mass m_i. Eventually, for $b_{\rm ho} = 0$ the particles can move only in the two dimensions of the xy plane.

As usual, the two-body wave function can be expanded in partial waves as

$$\Psi(\boldsymbol{r}) = \sum_{\ell m} \frac{u_\ell(r)}{r} Y_{\ell m}(\theta, \varphi), \tag{3}$$

where $\boldsymbol{r} = \boldsymbol{r}_1 - \boldsymbol{r}_2$ is the relative coordinate between the two particles whose direction is given by the polar and azimuthal angles θ and φ, respectively. For simplicity, in the notation we shall assume spinless particles, although the generalization to particles with nonzero spin is straightforward.

For two particles with masses m_1 and m_2 and coordinates $\boldsymbol{r}_1$ and $\boldsymbol{r}_2$ we have that

$$r^2 = \frac{m_1}{\mu} r_1^2 + \frac{m_2}{\mu} r_2^2 - \frac{m_1 + m_2}{\mu} r_{cm}^2, \tag{4}$$

where μ is the reduced mass and $\boldsymbol{r}_{cm}$ is the position of the two-body center of mass. This expression permits us to write the full trap potential as

$$\begin{aligned} &\tfrac{1}{2} m_1 \omega^2 r_1^2 \cos^2\theta_1 + \tfrac{1}{2} m_2 \omega^2 r_2^2 \cos^2\theta_2 \\ &\quad = \tfrac{1}{2} \mu \omega^2 r^2 \cos^2\theta + \tfrac{1}{2}(m_1 + m_2)\omega^2 r_{cm}^2 \cos^2\theta_{cm}, \end{aligned} \tag{5}$$

where θ_{cm} is the polar angle associated with $\boldsymbol{r}_{cm}$. The expression above implies that, after removal of the center-of-mass motion, the squeezing potential to be used in the relative two-body calculation takes the form

$$V_{\rm trap}(r, \theta) = \tfrac{1}{2} \mu \omega^2 r^2 \cos^2\theta, \tag{6}$$

whose ground-state energy is $E_{\rm ho} = \hbar\omega/2$.

The wave functions u_ℓ in Eq. (3) are the solutions of the radial Schrödinger equation

$$\begin{aligned} &\left[\frac{\partial^2}{\partial r^2} - \frac{\ell(\ell+1)}{r^2} - \frac{2\mu}{\hbar^2} V_{2b}(r) + \frac{2\mu E_{\rm tot}}{\hbar^2}\right] u_\ell \\ &\quad - \frac{2\mu}{\hbar^2} \sum_{\ell' m'} \langle Y_{\ell m} | V_{\rm trap}(r, \theta) | Y_{\ell' m'} \rangle_\Omega u_{\ell'} = 0, \end{aligned} \tag{7}$$

where $V_{2b}(r)$ is the two-body interaction (assumed to be central), $\langle\ \rangle_\Omega$ indicates integration over the angles only, and $E_{\rm tot}$ is the total relative two-body energy. The energy E of the two-body system will be obtained after subtraction of the harmonic oscillator energy, i.e., $E = E_{\rm tot} - \hbar\omega/2$.

An important point is that the squeezing potential (6) is not central, and therefore the orbital angular momentum quantum number, ℓ, is not conserved. In other words, the trap potential is not diagonal in $\ell\ell'$. In particular we have

$$\langle Y_{\ell m} | V_{\rm trap}(r, \theta) | Y_{\ell' m'} \rangle_\Omega = \tfrac{1}{2} \mu \omega^2 r^2 \langle Y_{\ell m} | \cos^2\theta | Y_{\ell' m'} \rangle_\Omega \tag{8}$$

and

$$\begin{aligned} &\langle Y_{\ell m} | \cos^2\theta | Y_{\ell' m'} \rangle_\Omega \\ &\quad = \delta_{m m'} (-1)^m \sum_L (2L+1) \sqrt{2\ell+1} \sqrt{2\ell'+1} \\ &\qquad \times \begin{pmatrix} 1 & 1 & L \\ 0 & 0 & 0 \end{pmatrix}^2 \begin{pmatrix} \ell & L & \ell' \\ 0 & 0 & 0 \end{pmatrix} \begin{pmatrix} \ell & L & \ell' \\ -m & 0 & m \end{pmatrix}, \end{aligned} \tag{9}$$

where the brackets are $3j$ symbols, L can then obviously only take the values $L = 0$ and $L = 2$, and therefore $\ell + \ell'$ has to be an even number (so, the parity is well defined). Note that the angular momentum projection m actually remains as a good quantum number throughout the transition to 2D. Therefore, the value taken for m in Eq. (9) characterizes the solution in 2D obtained after infinite squeezing.

In the 3D limit ($V_{\rm trap} = 0$) the partial waves decouple, and the 3D wave function has, of course, a well-defined orbital angular momentum. In the calculations reported in this work the 3D wave function will be assumed to have $\ell = 0$, which therefore means that $m = 0$.

Note that if we take $m_\omega = \mu$, and we make use of Eqs. (1) and (6), the coupled equations (7) can be written as

$$\begin{aligned} &\left[\frac{\partial^2}{\partial r_b^2} - \frac{\ell(\ell+1)}{r_b^2} - 2V_{2b}^b(r) + 2E_{\rm tot}^b\right] u_\ell \\ &\quad - \frac{r_b^2}{\left(b_{\rm ho}^b\right)^4} \sum_{\ell' m'} \langle Y_{\ell m} | \cos^2\theta | Y_{\ell' m'} \rangle_\Omega u_{\ell'} = 0, \end{aligned} \tag{10}$$

where, taking b as some convenient length unit, we have defined $r_b = r/b$, $b_{\rm ho}^b = b_{\rm ho}/b$, $V_{2b}^b = V_{2b}/(\hbar^2/\mu b^2)$, and $E_{\rm tot}^b = E_{\rm tot}/(\hbar^2/\mu b^2)$. In other words, when taking b and $\hbar^2/\mu b^2$ as length and energy units, respectively, the two-body radial equation, Eq. (10), is independent of the reduced mass of the system.

B. 2D → 1D

The confinement from two to one dimensions can be made in a way similar to that done in the previous subsection for the 3D → 2D case, that is, solving the two-dimensional two-body problem with an external squeezing potential along one direction (which we choose along the y axis).

As before, when working in the center-of-mass frame, the external potential will be given by

$$V_{\rm trap} = \tfrac{1}{2} \mu \omega^2 r^2 \sin^2\varphi, \tag{11}$$

where, as in Eq. (6), the radial coordinate r is the relative distance between the two particles, but where now the polar angle φ is such that $x = r\cos\varphi$ and $y = r\sin\varphi$. In this way, after infinite squeezing, the particles are allowed to move along the x axis only.

In 2D the partial wave expansion of the wave function, analogous to Eq. (3), is given by

$$\Psi(\boldsymbol{r}) = \sum_m \frac{u_m(r)}{\sqrt{r}} Y_m(\varphi), \tag{12}$$

where the angular functions

$$Y_m(\varphi) = \frac{1}{\sqrt{2\pi}} e^{im\varphi} \tag{13}$$

are the eigenfunctions of the 2D angular momentum operator $-i\hbar\partial/\partial\varphi$, whose eigenvalue $\hbar m$ can take positive and negative values, where m is an integer.

Using the expansion in Eq. (12), the 2D radial Schrödinger equation then reads

$$\begin{aligned} &\left[\frac{\partial^2}{\partial r^2} + \frac{\frac{1}{4} - m^2}{r^2} - \frac{2\mu}{\hbar^2} V_{2b}(r) + \frac{2\mu E_{\rm tot}}{\hbar^2}\right] u_m \\ &\quad - \frac{2\mu}{\hbar^2} \sum_{m'} \langle Y_m | V_{\rm trap}(r, \varphi) | Y_{m'} \rangle_\Omega u_{m'} = 0, \end{aligned} \tag{14}$$

which is equivalent to Eq. (7). Using Eq. (13), it is not difficult to see that

$$\langle Y_m|V_{\rm trap}(r,\varphi)|Y_{m'}\rangle_\Omega = \tfrac{1}{2}\mu\omega^2 r^2\langle Y_m|\sin^2\varphi|Y_{m'}\rangle_\Omega \quad (15)$$

and

$$\langle Y_m|\sin^2\varphi|Y_{m'}\rangle_\Omega = \tfrac{1}{2}\delta_{m,m'} - \tfrac{1}{4}\delta_{m,m'\pm 2}, \quad (16)$$

which implies that, as in the 3D → 2D case, the squeezing potential is again mixing different angular momentum quantum numbers.

The procedure shown up to here is completely analogous to the one described in the previous subsection for 3D → 2D squeezing. However, in this case the starting point is the 2D Schrödinger equation Eq. (14), which shows the important feature that for s waves ($m = 0$) the "centrifugal" barrier is actually attractive, and it takes the very particular form of $-1/4r^2$. This barrier happens to be precisely the critical potential giving rise to the "falling to the center" or Thomas effect [17]. As a consequence, the numerical resolution of the differential equation (14) can encounter difficulties associated with this pathological behavior.

To overcome this numerical problem, it is more convenient to face the 2D → 1D squeezing problem solving the Schrödinger equation directly in Cartesian coordinates:

$$\left[-\frac{\hbar^2}{2\mu}\left(\frac{\partial^2}{\partial x^2}+\frac{\partial^2}{\partial y^2}\right)+V(x,y)+V_{\rm trap}(y)-E_{\rm tot}\right]\Psi = 0. \quad (17)$$

This can be easily made after expanding the two-body relative wave function, Ψ, in an appropriate basis set where the Hamiltonian can be diagonalized. A possible choice for the basis could be $\{|\psi_{n_x}(x)\psi_{n_y}(y))\}$, with ψ_n being the harmonic oscillator eigenfunctions. Needless to say, solving either Eq. (14) or (17) is completely equivalent, although in (17) the problematic attractive barrier is not present, and the dependence on the angular momentum m also disappears.

Again, as discussed in Eq. (10), after taking $m_\omega = \mu$ in Eq. (1), and b and $\hbar^2/\mu b^2$ as length and energy units, respectively, Eq. (14) [or (17)] becomes μ independent.

C. 3D → 1D

If the confinement procedures 3D → 2D and 2D → 1D described in Secs. II A and II B are performed consecutively, we are then obviously performing a 3D → 1D squeezing, but going through an intermediate 2D geometry. However, this is not really necessary, since it is always possible to squeeze the system in two directions simultaneously, which will lead to the same 1D space but without going through the 2D configuration.

Let us consider that the particles, in principle moving in a 3D space, are confined be means of two external harmonic oscillator potentials acting on the x and the y directions simultaneously. The trap potential felt by each of the particles is then

$$V_{\rm trap}^{(i)} = \tfrac{1}{2}m_i\omega_x^2 x_i^2 + \tfrac{1}{2}m_i\omega_y^2 y_i^2, \quad (18)$$

where x_i and y_i are the x and y coordinates of particle i, and ω_x and ω_y are the harmonic oscillator frequencies of each of the two external potentials. These frequencies determine the independent squeezing on each of the directions, and of course the infinitely many possible values of the ω_x/ω_y ratio determine the infinitely many possible ways of squeezing from 3D into 1D.

Let us here consider the simplest case in which $\omega_x = \omega_y = \omega$. After using spherical coordinates, we trivially get that

$$V_{\rm trap}^{(i)} = \frac{1}{2}m_i\omega^2 r_i^2\sin^2\theta_i = \frac{1}{2}\frac{m_i\hbar^2}{m_\omega^2 b_{\rm ho}^4}r_i^2\sin^2\theta_i, \quad (19)$$

which, as one could expect, is identical to Eq. (2) but replacing $\cos\theta_i$ with $\sin\theta_i$. This simply means that the vector coordinate $\boldsymbol{r}_i$ is not projected on the z axis, but on the xy plane.

Therefore, the discussion below Eq. (2) still holds here, but replacing $\cos\theta$ with $\sin\theta$ all over, which leads again to Eq. (7) but where now

$$\langle Y_{\ell m}|V_{\rm trap}(r,\theta)|Y_{\ell' m'}\rangle_\Omega = \tfrac{1}{2}\mu\omega^2 r^2\langle Y_{\ell m}|\sin^2\theta|Y_{\ell' m'}\rangle_\Omega, \quad (20)$$

with

$$\langle Y_{\ell m}|\sin^2\theta|Y_{\ell' m'}\rangle_\Omega = \delta_{\ell\ell'}\delta_{mm'} - \langle Y_{\ell m}|\cos^2\theta|Y_{\ell' m'}\rangle_\Omega, \quad (21)$$

and where the last matrix element is given by Eq. (9).

Since in this case we have included two harmonic oscillator potentials, the energy provided by them, still assuming $\omega_x = \omega_y = \omega$, will be $E_{\rm ho} = \hbar\omega$, and therefore $E = E_{\rm tot} - \hbar\omega$.

III. TWO-BODY SYSTEMS IN d DIMENSIONS

An alternative to the continuous squeezing of the particles by means of external potentials can be to solve the two-body problem in d dimensions, where d can take any value within the initial and final dimensions ($3 \geqslant d \geqslant 2$, $2 \geqslant d \geqslant 1$, or $3 \geqslant d \geqslant 1$). The idea is that, given a squeezed system by means of an external potential with squeezing parameter $b_{\rm ho}$, it is then possible to associate this particular squeezing parameter to some specific noninteger value of the dimension, such that the properties of the system can be obtained by solving the, in general simpler, d-dimensional problem. The basic properties of two-body systems in d dimensions are described in Appendix C of Ref. [1]. For this reason, in this section we just collect the key equations relevant for the work presented here.

A. Theoretical formulation

Let us consider a two-body system where the relative coordinate between the two constituents is given by $\boldsymbol{r}$. In principle the components of the vector $\boldsymbol{r}$ in a d-dimensional space will be given by the d Cartesian coordinates $(r_1, r_2, \ldots, r_d)$. As is well known, when dealing with central potentials, it is however much more convenient to use the set of generalized spherical coordinates, which contain just one radial coordinate $r = \sqrt{r_1^2 + r_2^2 + \cdots + r_d^2}$ and $d-1$ angles (for instance the polar and azimuthal angles when $d = 3$). In this way, the two-body wave function can be expanded in terms of the generalized d-dimensional spherical harmonics, which depend on the $d-1$ angles (see [1] for details):

$$\Psi_d(\boldsymbol{r}) = \frac{1}{r^{\frac{d-1}{2}}}\sum_\nu R_\nu^{(d)}(r)Y_\nu(\Omega_d), \quad (22)$$

where ν represents the summation over all the required quantum numbers, Ω_d collects the $d-1$ angular coordinates, and where $\int Y_\nu^* Y_{\nu'} d\Omega_d = \delta_{\nu\nu'}$.

Of course, what is written above makes full sense provided that d takes integer values. However, when d is not an integer, which obviously will happen when changing the dimension continuously from the initial down to the final dimension, the meaning of the $d-1$ angles in Eq. (22) is not obvious. Nevertheless, in this work we are not having this problem, since we are considering relative s waves only, which implies that the wave function (22) is angle independent, and it can actually be written as

$$\Psi_d(\boldsymbol{r}) = \frac{1}{r^{(d-1)/2}} R_d(r) Y_d, \tag{23}$$

where the constant s-wave spherical harmonic, Y_d, can be obtained simply by keeping in mind that in d dimensions we have that [18]

$$\int d\Omega_d = \frac{2\pi^{d/2}}{\Gamma\left(\frac{d}{2}\right)}, \tag{24}$$

which, making use of the fact that $Y_d^* Y_d \int d\Omega_d = 1$, immediately leads to

$$Y_d = \left[\frac{\Gamma\left(\frac{d}{2}\right)}{2\pi^{d/2}}\right]^{1/2}. \tag{25}$$

Finally, the radial wave function, $R_d(r)$, in Eq. (23) is obtained as the solution of the d-dimensional radial Schrödinger equation, which for s waves reads [1]

$$\left\{\frac{\partial^2}{\partial r^2} - \frac{\frac{1}{4}(d-3)(d-1)}{r^2} - \frac{2\mu}{\hbar^2}[V_{2b}(r) - E]\right\} R_d(r) = 0, \tag{26}$$

where, since the only potential entering is just the two-body interaction, the energy E is the true two-body relative energy.

It is important to note that if we write $d = 2 + x$ with $-1 \leqslant x \leqslant 1$, the barrier in Eq. (26) takes the form $(x^2-1)/4r^2$, which indicates that the equation to be solved is the same for $d = 2 - x$ and $d = 2 + x$. This might suggest that the bound-state solutions of Eq. (26) should be symmetric around $d = 2$. For instance, for $d = 1$ and $d = 3$ the barrier disappears, and one could expect the same solution in the two cases. However, as discussed below, this is not really like this.

Note that the centrifugal barrier in Eq. (26) can also be written in the usual way, $\ell^*(\ell^*+1)/r^2$, simply by defining $\ell^* = (d-3)/2$. This means that Eq. (26) is formally identical to the usual radial two-body Schrödinger equation with angular momentum ℓ^*. Therefore, as is well known, Eq. (26) has in general two possible solutions, each of them associated with a different short-distance behavior:

$$R_d^{(1)}(kr) \overset{kr\to 0}{\longrightarrow} kr j_{\ell^*}(kr) \overset{kr\to 0}{\longrightarrow} r^{\ell^*+1} = r^{\frac{d-1}{2}}, \tag{27}$$

$$R_d^{(2)}(kr) \overset{kr\to 0}{\longrightarrow} kr \eta_{\ell^*}(kr) \overset{kr\to 0}{\longrightarrow} r^{-\ell^*} = r^{\frac{3-d}{2}}, \tag{28}$$

where j_{ℓ^*} and η_{ℓ^*} are the regular and irregular spherical Bessel functions, respectively, and $k = \sqrt{2\mu|E|}/\hbar$. Within the dimension range $1 \leqslant d \leqslant 3$, these two radial solutions go to zero for $kr \to 0$, except for $d = 1$ and $d = 3$, where one of the solutions goes to a constant value.

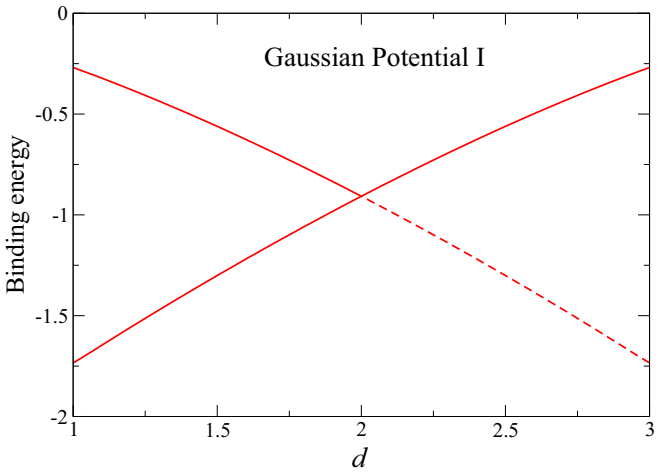

FIG. 1. Binding energies obtained from Eq. (26) as a function of d. The two-body potential used is the Gaussian potential indicated as potential I in Table I. The dashed line corresponds to the states to be discarded due to the divergence of the solution at the origin.

However, as shown in Eq. (23), the full radial wave function is actually $R_d(r)/r^{(d-1)/2}$. After dividing by the phase space factor we immediately see that the solution in Eq. (27) leads to a constant value of the full radial wave function at $r = 0$ no matter the dimension d. Thus, the solution (27) is valid in the full dimension range $1 \leqslant d \leqslant 3$. However, after dividing by the phase space factor, the radial solution obtained from Eq. (28) behaves at short distances as r^{2-d}. This means that this solution is regular at the origin only for $d < 2$, whereas it has to be disregarded for $d > 2$. For $d > 2$ only the solution (27), whose short-distance behavior is determined by the regular Bessel function, is physically acceptable.

Therefore the apparent symmetry of Eq. (26) around $d = 2$ is not real. The two-body problem has two solutions with physical meaning for $d < 2$, and only one for $d > 2$. Furthermore, the solution to be disregarded for $d > 2$ corresponds to a larger binding, which implies that the ground state of the system will be more bound for $d = 1$ than for $d = 3$. This is illustrated in Fig. 1, where we show the two computed binding energies arising from Eq. (26) as a function of the dimension d.

Although not relevant at this stage, let us mention for completeness that the two-body potential used in the calculation is the one that later on will be called Gaussian potential I. The branch indicated in Fig. 1 by the dashed curve for $d > 2$ is the one obtained after imposing on the solution the short-distance behavior (28), which, as discussed above, cannot be accepted as a physical solution due to the divergence of the full radial wave function at the origin. As seen also in the figure, for $d = 2$ the two solutions merge into a single one, as expected due to the fact that the short-distance behavior (27) and (28) is the same in this case.

B. Interpretation of the wave function

Once the d-dimensional radial wave function, $R_d(r)$, has been obtained, it is possible to compute different observables in d dimensions, as for instance the root-mean-square radius,

which is given by the simple expression

$$r_d^2 = \int_0^\infty r^2 |R_d(r)|^2 dr. \tag{29}$$

However, the reliability of a direct use of a noninteger d-dimensional wave function, Ψ_d, to compute a given observable, which unavoidably is measured in a three- or two-dimensional space, is not obvious. It could actually look more convenient to use instead the wave function obtained with an external squeezing potential, which, although very often more difficult to compute, is, in the strict sense, a three- or two-dimensional wave function.

In order to exploit the simplicity in the calculation of the Ψ_d wave function, it is necessary to obtain a procedure to translate the noninteger d-dimensional wave function into the ordinary three- or two-dimensional space.

To do so, let us start by noticing that a squeezing of the system by an external field acting along one (for the 3D→2D and 2D → 1D cases) or two (for the 3D → 1D case) directions necessarily proceeds through deformed structures in the initial dimension. It appears then necessary to provide a reinterpretation of the total spherical wave function in d dimensions, Ψ_d, as corresponding to a deformed three-dimensional system (for the 3D → 2D and 3D → 1D cases), or a deformed two-dimensional system (for the 2D → 1D case). The simplest way to account for this is to deform the radial coordinate r along the squeezed direction(s). In this way, if we consider the usual Cartesian coordinates $\{x, y, z\}$ for an initial 3D system, or the $\{x, y\}$ coordinates for an initial 2D system, we can interpret Ψ_d as an ordinary three- or two-dimensional wave function, but where the radial argument, r, is replaced by $\tilde{r}$, which is defined as

$$r \to \tilde{r} \equiv \sqrt{x^2 + y^2 + (z/s)^2} \equiv \sqrt{r_\perp^2 + (z/s)^2}, \tag{30}$$

$$r \to \tilde{r} \equiv \sqrt{(x^2 + y^2)/s^2 + z^2} \equiv \sqrt{(r_\perp/s)^2 + z^2}, \tag{31}$$

$$r \to \tilde{r} \equiv \sqrt{x^2 + (y/s)^2}, \tag{32}$$

for the 3D → 2D, 3D → 1D, and 2D → 1D cases, respectively.

In the expressions above, s is a scale parameter, assumed to be independent of the value of the squeezed coordinate, and which, in principle, lies within the range $0 \leqslant s \leqslant 1$. For $s = 1$, the relative radial coordinate $\tilde{r}$ is the usual one in spherical or polar coordinates, and the system is not deformed. For $s = 0$, only $z = 0$ in Eq. (30), $r_\perp = 0$ in Eq. (31), and $y = 0$ in Eq. (32) are possible; otherwise $\tilde{r} = \infty$ no matter the value of the nonsqueezed coordinate, and, since we are dealing with bound systems, $\Psi_d(\tilde{r}) = \Psi_d(\infty) = 0$. Therefore, the $s = 0$ situation corresponds to a completely squeezed system into two dimensions when (30) is used (3D → 2D), or into one dimension when (31) or (32) is used (3D → 1D or 2D → 1D).

It is important to note that after the transformation of the radial coordinate as defined in Eqs. (30) to (32), the d-dimensional wave function, Ψ_d, has to be normalized in the new three-dimensional space for the 3D → 2D and 3D → 1D cases:

$$2\pi \int r_\perp dr_\perp dz |\tilde{\Psi}_d(r_\perp, z, s)|^2 = 1, \tag{33}$$

or in the new two-dimensional space for the 2D → 1D case:

$$\int dxdy |\tilde{\Psi}_d(x, y, s)|^2 = 1, \tag{34}$$

where $\tilde{\Psi}_d \propto \Psi_d$ denotes the normalized wave function.

With this interpretation, where $\tilde{\Psi}_d$ is a wave function in the ordinary 3D (or 2D) space, one can obtain the expectation value of any observable $\mathcal{F}(\boldsymbol{r})$ in the usual way, that is,

$$\langle \mathcal{F}(\boldsymbol{r}) \rangle_s = \int r_\perp dr_\perp dz d\varphi \mathcal{F}(\boldsymbol{r}) |\tilde{\Psi}_d(r_\perp, z, s)|^2 \tag{35}$$

or

$$\langle \mathcal{F}(\boldsymbol{r}) \rangle_s = \int dxdy \mathcal{F}(\boldsymbol{r}) |\tilde{\Psi}_d(x, y, s)|^2. \tag{36}$$

The remaining point here is how to determine the value of the scale parameter, s, corresponding to a specific squeezing produced by an external field with a given oscillator parameter, $b_{\rm ho}$. The interpretation of Ψ_d as an ordinary (deformed) wave function using a constant s is very tempting. We believe this must be correct to leading order. If the Schrödinger equations are approximately solved by variation using single-Gaussian solutions we can directly identify the matching scale factor s. For instance, in case of squeezing along the z direction, the two single-Gaussian solutions will have the form $R_{ext} \propto e^{-r_\perp^2/2b^2 - z^2/2b_z^2}$ when the external field is used, and $R_d \propto e^{-r^2/2b_d^2}$ after the d calculation. If, following Eq. (30), we interpret R_d as a function of $\tilde{r}$, we easily get that R_{ext} and R_d are the same if $b = b_d$ and $s = b_z/b_d$. One way to improve is to allow s to be a function of the squeezed coordinate. The assumption is mostly that this dependence on the squeezed coordinate is rather smooth, in such a way that the function can be safely expanded around some constant average value, which therefore is the leading term.

In any case, the scale parameter s has to be a function of the noninteger dimension parameter, d, or equivalently, the squeezing length parameter, $b_{\rm ho}$. The value of the average scale parameter, s, then has to be obtained by comparison of the wave functions from a full external field, $\Psi_{b_{\rm ho}}(r)$, with $r^2 = r_\perp^2 + z^2$ (when squeezing from 3D) or $r^2 = x^2 + y^2$ (when squeezing from 2D), and the normalized d-dimensional wave function, $\tilde{\Psi}_d(\tilde{r})$, defined above.

Being more precise, we define the overlaps:

$$\mathcal{O}_{\rm 3D}(s) = 2\pi \int r_\perp dr_\perp dz \tilde{\Psi}_d(r_\perp, z, s) \Psi_{b_{\rm ho}}(r) \tag{37}$$

and

$$\mathcal{O}_{\rm 2D}(s) = \int dxdy \tilde{\Psi}_d(x, y, s) \Psi_{b_{\rm ho}}(r), \tag{38}$$

which are valid for initial 3D and 2D spaces, respectively. The scale parameter, s, is then determined such that the overlap (37) for the 3D → 2D and 3D → 1D cases, or the overlap (38) for the 2D → 1D case, is maximum.

In the Appendix we show, Eqs. (A7), (A12), and (A16), that the scale factor, s, is actually given by

$$s = \left(\frac{\langle z^2 \rangle_s}{\langle z^2 \rangle_{s=1}} \right)^{1/2}, \quad s = \left(\frac{\langle r_\perp^2 \rangle_s}{\langle r_\perp^2 \rangle_{s=1}} \right)^{1/2}, \quad s = \left(\frac{\langle y^2 \rangle_s}{\langle y^2 \rangle_{s=1}} \right)^{1/2}, \tag{39}$$

for the 3D → 2D, 3D → 1D, and 2D → 1D squeezing cases, respectively, where $\langle\ \rangle_s$ are expectation values as defined in Eqs. (35) and (36). This result says that s is nothing but the ratio between the expectation value of the squeezing coordinate for that value of s, and the one obtained without deforming the wave function ($s = 1$). These expressions make evident that the scale parameter, s, is a measure of the deformation along the squeezing direction(s).

IV. LARGE SQUEEZING REGIME

The large-squeezing region corresponds to very small values of the oscillator parameter, $b_{\rm ho}$, which implies that the squeezing potential dominates over the two-body interaction along the squeezing direction(s). As a consequence, the root-mean-square value of a given squeezed coordinate u is, for large squeezing, essentially given by the one corresponding to the harmonic oscillator potential. In particular this implies that, for a squeezing process d_iD → d_fD, we can write, in a compact way,

$$u_{\rm rms} = \langle u^2\rangle^{1/2} \overset{b_{\rm ho}\to 0}{\longrightarrow} \sqrt{\frac{d_i - d_f}{2}}\, b_{\rm ho}, \tag{40}$$

where u can be z, $r_\perp$, or y for the 3D → 2D, 3D → 1D, and 2D → 1D cases, respectively, and d_i and d_f indicate the initial and final dimension.

Let us now focus on the radius, r_d, defined in Eq. (29). To simplify ideas, let us consider first the case of a 3D → 2D squeezing along the z coordinate, and write r_d as

$$r_d^2 = \langle r^2\rangle = \langle r_\perp^2\rangle + \langle z^2\rangle. \tag{41}$$

Since the squeezing takes place along the z direction, the expectation value $\langle z^2\rangle$ is the one feeling the squeezing effect, whereas $\langle r_\perp^2\rangle$ to leading order does not. Following Eq. (39) we can then write

$$r_d^2 = \langle r_\perp^2\rangle + s^2\langle z^2\rangle_{s=1}, \tag{42}$$

where $\langle z^2\rangle_{s=1}$ is the expectation value of $\langle z^2\rangle$ when Ψ_d is interpreted as a non-deformed standard 3D wave function. Furthermore, for a spherical 3D wave function we know that $\langle x^2\rangle = \langle y^2\rangle = \langle z^2\rangle$, which means that $\langle r_\perp^2\rangle = \langle x^2\rangle + \langle y^2\rangle = 2\langle z^2\rangle_{s=1}$, and we can then write

$$r_d = \sqrt{2+s^2}\langle z^2\rangle_{s=1}^{1/2} = \frac{\sqrt{2+s^2}}{s}\langle z^2\rangle^{1/2}, \tag{43}$$

for 3D → 2D, where Eq. (39) has again been used.

The same argument is valid for the 3D → 1D case, except for the fact that now in Eq. (41) the squeezing is felt by $\langle r_\perp^2\rangle$ and not by $\langle z^2\rangle$. Therefore, using again Eq. (39), we can write $\langle r_\perp^2\rangle = s^2\langle r_\perp^2\rangle_{s=1}$, and $\langle z^2\rangle = \langle r_\perp^2\rangle_{s=1}/2$. In this way we get, for 3D → 1D,

$$r_d = \sqrt{\frac{1+2s^2}{2}}\langle r_\perp^2\rangle_{s=1}^{1/2} = \sqrt{\frac{1+2s^2}{2s^2}}\langle r_\perp^2\rangle^{1/2}. \tag{44}$$

Finally, similar arguments for the 2D → 1D case, where $r_d^2 = \langle r^2\rangle = \langle x^2\rangle + \langle y^2\rangle$, assuming the squeezing along y, lead to

$$r_d = \sqrt{1+s^2}\langle y^2\rangle_{s=1}^{1/2} = \frac{\sqrt{1+s^2}}{s}\langle y^2\rangle^{1/2}. \tag{45}$$

From Eqs. (43), (44), and (45) it is easy to obtain that, to leading order,

$$s \approx \sqrt{\frac{d_f}{d_i - d_f}}\,\frac{u_{\rm rms}/r_d}{\sqrt{1-(u_{\rm rms}/r_d)^2}}, \tag{46}$$

where $u_{\rm rms} \equiv \langle u^2\rangle^{1/2}$, and u represents either z, $r_\perp$, or y, depending on what squeezing process we are dealing with.

At this point it is easy to replace in Eq. (46) the large squeezing behavior of $\langle z^2\rangle$, $\langle r_\perp^2\rangle$, and $\langle y^2\rangle$ given in Eq. (40), and obtain the following expression for the scale parameter, s, in the case of large squeezing:

$$s \overset{b_{\rm ho}\to 0}{\longrightarrow} \left[\frac{d_f\left(\frac{b_{\rm ho}}{r_d}\right)^2}{2-(d_i-d_f)\left(\frac{b_{\rm ho}}{r_d}\right)^2}\right]^{1/2}, \tag{47}$$

where d_i and d_f again denote the initial and final dimension.

V. POTENTIALS

Let us start the numerical illustration by first specifying the chosen potentials along with a few of their characteristic properties. In the following subsections we continue to present results of the two methods described formally in Secs. II and III.

A. General properties

To allow general and hopefully universal conclusions, we shall use two different radial shapes for the two-body potential: a Gaussian potential, $V_{2b}(r) = S_g e^{-r^2/b^2}$, and a Morse-like potential, $V_{2b}(r) = S_m(e^{-2r/b} - 2e^{-r/b})$. The range of the interaction, b, will be taken as the corresponding (in principle different) length unit. Therefore, as discussed in Sec. II A, taking $m_\omega = \mu$ in Eq. (1) and $\hbar^2/\mu b^2$ as the energy unit, the Schrödinger equation is independent of the reduced mass.

For each of the potential shapes, three different interactions will be considered, potentials I, II, and III. The potential parameters for each of them are chosen such that the 3D scattering length, $a_{\rm 3D}$, is the same for both the Gaussian and the Morse shapes. The $a_{\rm 3D}$ values are in all the cases positive (therefore holding a 3D bound state), and change from comparable to the potential range, b, for potential I, to about 20 times b for potential II, and up to a value of about 40 times b for potential III.

The details of the potentials are given in Table I for the employed Gaussian and Morse shapes, where the lengths are in units of b, and the energies, including the strengths, S_g and S_m, are in units of $\hbar^2/\mu b^2$. The characterizing s-wave scattering lengths, $a_{\rm 3D}$, $a_{\rm 2D}$, and $a_{\rm 1D}$, are obtained in three-dimensional, two-dimensional, and one-dimensional calculations, respectively. The two-dimensional scattering length $a_{\rm 2D}$ is defined as given in Eq. (C6) in Ref. [1]. Furthermore, we give in Table I the corresponding s-wave ground-state binding energies, $E_{\rm 3D}$, $E_{\rm 2D}$, and $E_{\rm 1D}$, together with their root-mean-square radii, $r_{\rm 3D}$, $r_{\rm 2D}$, and $r_{\rm 1D}$.

All the potentials given in Table I give rise to only one bound state, i.e., the ground state. The only exception is potential I with Morse shape in one dimension. The two-body system described by this potential has a weakly bound excited

TABLE I. Strengths corresponding to the three Gaussian, S_g, and Morse, S_m, potentials used. For each of them we give the s-wave two-body binding energies of the ground state in three, two, and one dimensions (E_{3D}, E_{2D}, and E_{1D}), the corresponding s-wave scattering lengths a_{3D}, a_{2D}, and a_{1D}, and the root-mean-square radii r_{3D}, r_{2D}, and r_{1D}. All the energies are given in units of $\hbar^2/\mu b^2$ and the lengths in units of b, where b is the range of either the Gaussian or the Morse potential.

	Potential I	Potential II	Potential III
S_g	−2.71	−1.43	−1.38
E_{3D}	−0.269	-1.651×10^{-3}	-3.144×10^{-4}
E_{2D}	−0.908	−0.269	−0.249
E_{1D}	−1.734	−0.771	−0.736
a_{3D}	2.033	18.122	40.598
a_{2D}	1.103	1.883	1.942
a_{1D}	0.063	0.899	0.928
r_{3D}	1.508	12.823	28.710
r_{2D}	0.926	1.398	1.439
r_{1D}	0.572	0.747	0.759
S_m	1.294	0.474	0.434
E_{3D}	−0.189	-1.875×10^{-3}	-3.325×10^{-4}
E_{2D}	−0.450	-7.394×10^{-2}	-6.088×10^{-2}
E_{1D}	−0.811	−0.228	−0.203
a_{3D}	2.033	18.122	40.598
a_{2D}	$\sim10^{-8}$	3.536	3.872
a_{1D}	14.0	0.986	1.243
r_{3D}	2.235	12.870	28.741
r_{2D}	1.458	2.739	2.947
r_{1D}	0.875	1.366	1.428

state, such that the large value of the scattering length a_{1D} is in this case related to the appearance of this second state, whose energy can be approximated by some constant divided by a_{1D}^2 (Eq. (C9) in Ref. [1]).

B. External harmonic oscillator potential

Let us start with the case of confinement by means of an external (harmonic oscillator) potential. The procedure is as described in Sec. II, where it is shown how the trap potential, which is not central, mixes different values of the relative orbital angular momentum. This is made evident in Eqs. (9), (16), and (21) for the three different squeezing processes (3D → 2D, 2D → 1D, 3D → 1D) considered in this work. Therefore, it is not difficult to foresee that the stronger the squeezing, the larger the number of terms in the expansions (3) and (12) required to get convergence. In fact, for no squeezing, the orbital angular momentum is a good quantum number and only one term in the expansion enters.

In order to illustrate the pattern of convergence, let us consider the 3D → 2D case and call ℓ_{max} the maximum value of ℓ included in the expansion (3). In Fig. 2(a) we show the convergence of the two-body energy as a function of ℓ_{max} for the Gaussian potential I (Table I), and for different values of $b^b_{ho} = b_{ho}/b$ in the squeezing potential. The energy shown, E, is the two-body energy obtained after subtracting the harmonic oscillator energy, i.e., $E = E_{tot} - E_{ho}$. The horizontal

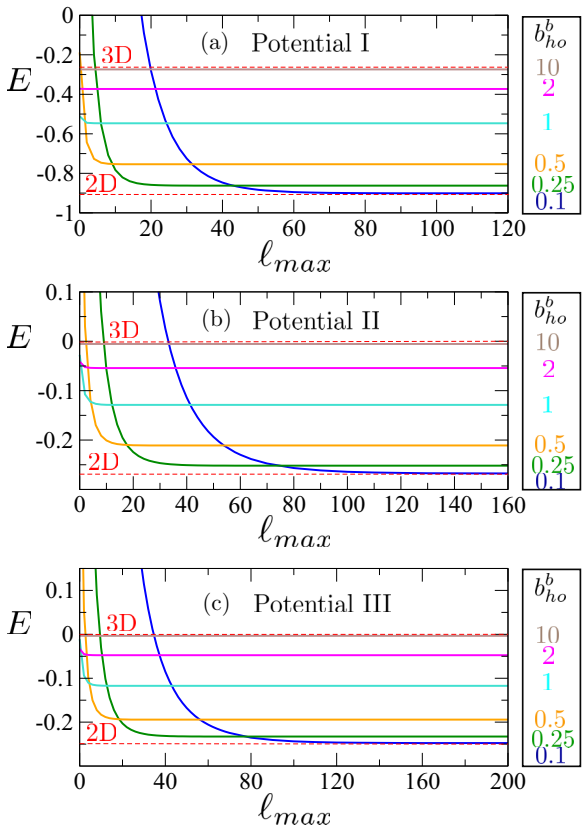

FIG. 2. Two-body energies (after subtracting the harmonic oscillator energy), in units of $\hbar^2/\mu b^2$, for the Gaussian potentials in a 3D → 2D squeezing, as a function of the ℓ_{max} value included in the expansion (3). The results for $b^b_{ho} = b_{ho}/b = 0.1$, 0.25, 0.5, 1, 2, and 10 are shown. Panels (a), (b), and (c) refer to potentials I, II, and III, respectively. In each panel, the upper and lower horizontal dashed lines indicate the two-body energies in the 3D and 2D cases, respectively, as indicated by the "3D" and "2D" labels.

dashed lines are the two-body energies obtained after a 3D and a 2D calculation, respectively, which are given in Table I.

As expected, for small values of the oscillator parameter we recover the computed 2D energy, whereas for large values of b^b_{ho} the 3D energy is approached. We can also see that the smaller b^b_{ho}, the larger the ℓ_{max} value needed to get convergence. Partial waves with ℓ values up to around 80 are at least needed for $b^b_{ho} = 0.1$, for which we get a converged energy of −0.901, pretty close to the value of −0.908 obtained in a 2D calculation. For large values of b^b_{ho} the convergence is obviously much faster. For $b^b_{ho} = 10$ we obtain an energy of −0.274, not far from the value of −0.269 corresponding to the 3D calculation. This result is already obtained including the $\ell = 0$ component only.

In Fig. 2(b) we show the same as in Fig. 2(a) for the Gaussian potential II. The general features are the same as before, although there are some remarkable differences arising from the fact that now the scattering length is about 9 times bigger. First, for $b^b_{ho} = 10$ we obtain a converged energy of -5.43×10^{-3}, which, although in the figure seems to be very close to 3D energy, differs by more than a factor of three ($E_{3D} = -1.65\times10^{-3}$). To get a better agreement with the 3D energy, b^b_{ho} values of a few times the 3D scattering

length are needed (as in fact observed for potential I). The second important difference is that convergence is now slower than before, and higher values of $\ell_{\max}$ are needed to get convergence for small oscillator lengths.

These facts are more emphasized when using the Gaussian potential III, whose corresponding curves are shown in Fig. 2(c). In this case we have obtained for $b^b_{\rm ho} = 10$ a converged energy of -3.41×10^{-3}, about an order of magnitude more bound than the 3D energy (-3.14×10^{-4}). For $b^b_{\rm ho} = 0.1$, an $\ell_{\max}$ value of at least 140 is needed in order to get convergence. This is of course related to the large 3D scattering length. In three dimensions the bound two-body system is clearly bigger than with the other two potentials, and, consequently, it starts feeling the confinement sooner than in the other cases.

The convergence features for 2D $\to$ 1D and 3D $\to$ 1D confinement, as well as for the Morse potentials, are the same as the ones described in Fig. 2, namely, for large values of $b^b_{\rm ho}$ (little squeezing) a small number of partial waves is enough to get convergence and the energy in the initial dimension, 2D or 3D, is approached, whereas for small values of $b^b_{\rm ho}$ (large squeezing) a higher number of partial waves is required, and the energy in the final dimension, 1D or 2D, is recovered. For this reason we consider it to be unnecessary to show the corresponding figures. In any case, as discussed in Sec. II B, for 2D $\to$ 1D squeezing it is more convenient to solve directly Eq. (17), where the partial wave expansion does not enter explicitly.

In Figs. 3(a), 3(b), and 3(c) we show, for the 3D $\to$ 2D, 2D $\to$ 1D, and 3D $\to$ 1D cases, respectively, the converged values of the two-body energy E for the Gaussian potentials (thick curves) and the Morse potentials (thin curves), as a function of the oscillator parameter, $b^b_{\rm ho}$. The energy is normalized to the energy in the final dimension, either $E_{\rm 2D}$ or $E_{\rm 1D}$, given in Table I. Therefore, for small values of $b^b_{\rm ho}$ all the curves go to 1.

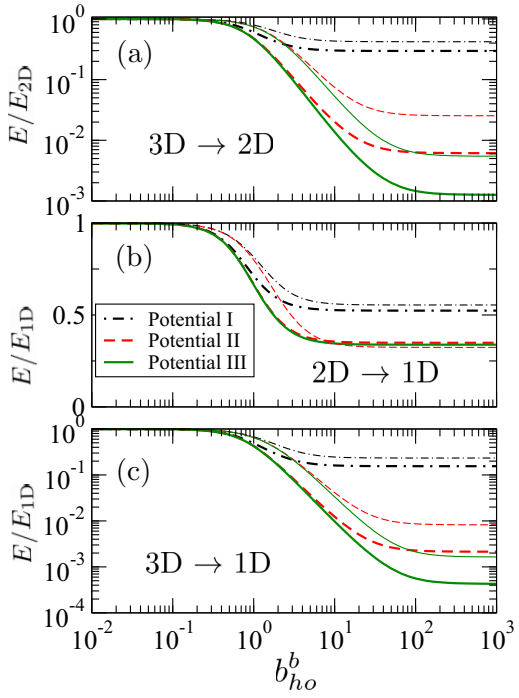

FIG. 3. Converged two-body energies (normalized to the energy in the final dimension) for the three Gaussian (thick curves) and Morse (thin curves) potentials as a function of $b^b_{\rm ho}$. Panels (a), (b), and (c) correspond to 3D $\to$ 2D, 2D $\to$ 1D, and 3D $\to$ 1D squeezing, respectively.

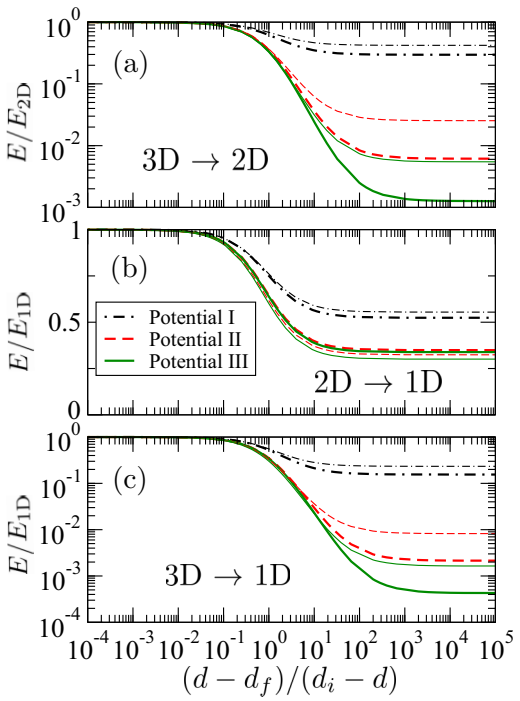

FIG. 4. Two-body energies (normalized to the energy in the final dimension) for the three Gaussian (thick curves) and the three Morse (thin curves) potentials used as a function of $(d-d_f)/(d_i-d)$, where d is the dimension varying continuously from the initial dimension d_i to the final dimension d_f. Panels (a), (b), and (c) correspond to 3D $\to$ 2D, 2D $\to$ 1D, and 3D $\to$ 1D squeezing, respectively.

C. Two-body energy in d dimensions

As described in Sec. III, the continuous squeezing of the system from some initial dimension d_i to some final dimension d_f can also be made by solving the two-body problem in d dimensions, where $d_f \leqslant d \leqslant d_i$. We can therefore compute the same observable as in Fig. 3 but solving the two-body Schrödinger equation (26), where the dimension d is taken as a parameter. It is important to remember that for $d > 2$ the ground-state solution behaves for $\kappa r \to 0$ as given in Eq. (27), whereas for $d < 2$ the ground state follows the behavior given by Eq. (28).

The results are shown in Fig. 4 as a function of $(d-d_f)/(d_i-d)$ for the squeezing cases 3D $\to$ 2D [panel (a)], 2D $\to$ 1D [panel (b)], and 3D $\to$ 1D [panel (c)]. Again, the thick and thin curves correspond to the results with the Gaussian and Morse potentials, respectively. The choice of the abscissa coordinate is such that the curves can be easily compared to the ones in Fig. 3. In fact, a simple eye inspection of both figures makes evident the existence of a univocal connection between $b^b_{\rm ho}$ and d.

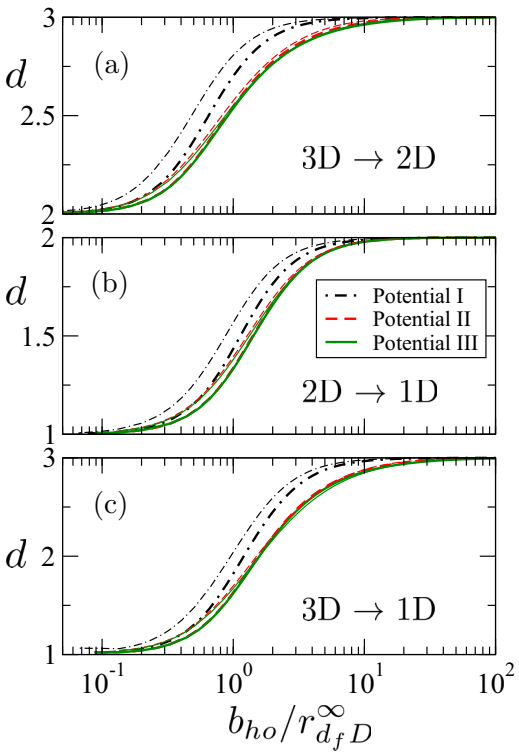

FIG. 5. Values of d as a function of $b_{\rm ho}/r^{\infty}_{d_f{\rm D}}$, obtained by matching the energies in Figs. 3 and 4, for the potentials in Table I. The cases of 3D → 2D, 2D → 1D, and 3D → 1D squeezing are shown in panels (a), (b), and (c), respectively. The thick and thin dashed curves correspond to the results obtained for the Gaussian and Morse potentials, respectively. The radius $r^{\infty}_{d_f{\rm D}}$ is the root-mean-square radius in the final dimension, d_f, obtained with a potential such that $a_{\rm 3D} = \infty$.

VI. COMPARING THE TWO METHODS

Although the parameters used in each of the two methods, $b_{\rm ho}$ and d, have a very different nature, they both are used to describe the same physics process of squeezing the system into a lower-dimensional space. We shall first connect these parameters by use of the energies leading from initial to final dimension in the squeezing processes. Then we turn to the crucial comparison of the related wave functions which require an interpretation and a deformation parameter, as described in Sec. III B.

A. Relation between $b^b_{\rm ho}$ and d

The relation between $b^b_{\rm ho}$ and d obtained directly from Figs. 3 and 4 is shown in Fig. 5 for all the potentials. Panels (a), (b), and (c) correspond to the 3D → 2D, 2D → 1D, and 3D → 1D cases, respectively. As in the previous figures, the thick and thin curves are, respectively, the results obtained with the Gaussian and Morse potentials.

In the figure we show d as a function of $b_{\rm ho}/r^{\infty}_{d_f{\rm D}}$, where $r^{\infty}_{d_f{\rm D}}$ is the root-mean-square radius of the bound two-body system in the final dimension obtained with an interaction such that $a_{\rm 3D} = \infty$. In particular $r^{\infty}_{\rm 1D}$ and $r^{\infty}_{\rm 2D}$ take the values 0.769 and 1.474, in units of b, for the Gaussian shape, and 1.478 and 3.128 for the Morse shape, respectively. This is a way to normalize the size of the bound state in the final dimension, d_f, to the value corresponding to the potential, which, in principle, is expected to provide a universal connection between d and $b_{\rm ho}$. In fact, as shown in the figure, for each of the two potential shapes, the curves corresponding to the potentials with large scattering length, potentials II and III, are almost identical to each other. Furthermore, the curves for these two potentials corresponding to the Gaussian (thick curves) and Morse (thin curves) potentials are not very different. Only the cases corresponding to potential I give rise to curves clearly different from the other ones.

This result is consistent with the idea of relating universal properties of quantum systems to the presence of relative s waves and large scattering lengths. This has been established as a universal parameter describing properties of weakly bound states without reference to the responsible short-range attraction. For this reason, the translation between $b_{\rm ho}$ and d shown in Fig. 5 for the potentials with large scattering length should be very close to the desired universal relation between the two parameters.

B. Scale parameter

As discussed in Sec. III B, the wave function in d dimensions can be interpreted as an ordinary wave function in three dimensions (in the 3D → 2D or 3D → 1D cases) or in two dimensions (in the 2D → 1D case), but with a deformation along the squeezing direction, as shown in Eqs. (30), (31), and (32). The value of the scale parameter, s, is obtained as the one maximizing the overlap, $\mathcal{O}_{\rm 3D}$, in Eq. (37) for the 3D → 2D or 3D → 1D cases, or the overlap, $\mathcal{O}_{\rm 2D}$, in Eq. (38) for the 2D → 1D case. These overlaps, which are functions of the scale parameter, s, are just the overlap between the wave function obtained with the external squeezing potential, $\Psi_{b_{\rm ho}}$, and the renormalized wave function, $\tilde{\Psi}_d$, obtained in d dimensions, where $b_{\rm ho}$ and d are related as shown in Fig. 5.

The results obtained for the scale parameter are shown in Fig. 6 for the three squeezing processes and the usual three potentials for both the Gaussian (thick curves) and Morse (thin curves) shapes. In all the cases the maximized overlap value is very close to 1. In fact, in the most unfavorable computed case ($b^b_{\rm ho} = 0.1$), the overlap value is, for all the cases, at least 0.98. As expected, a large squeezing ($b^b_{\rm ho} \to 0$) implies a small value of s ($s \to 0$), whereas a small squeezing (large $b^b_{\rm ho}$) corresponds to $s \to 1$. In fact, for $b_{\rm ho} = \infty$, Eqs. (7) and (14) are identical to Eq. (26) for $d = 3$ and $d = 2$, respectively. This means that the wave functions, $\Psi_{b_{\rm ho}}$ and Ψ_d, are identical, and the corresponding overlaps, $\mathcal{O}_{\rm 3D}$ or $\mathcal{O}_{\rm 2D}$, are trivially maximized and equal to 1 for $s = 1$.

Another feature observed in Fig. 6 is that when the squeezing begins, for relatively large values of $b^b_{\rm ho}$, the scale parameter, s, can be bigger than 1. This is especially true for potentials II and III in the 3D → 1D squeezing. This fact indicates that in this region (d very close to the initial dimension) the interpretation of the d-wave function as the three-dimensional wave function, $\tilde{\Psi}_d(\tilde{r})$, gives rise to a state with the particles a bit too confined along the squeezing direction, in such a way that maximization of the overlap (37) or (38) requires a small release of the confinement by means of a scale factor bigger

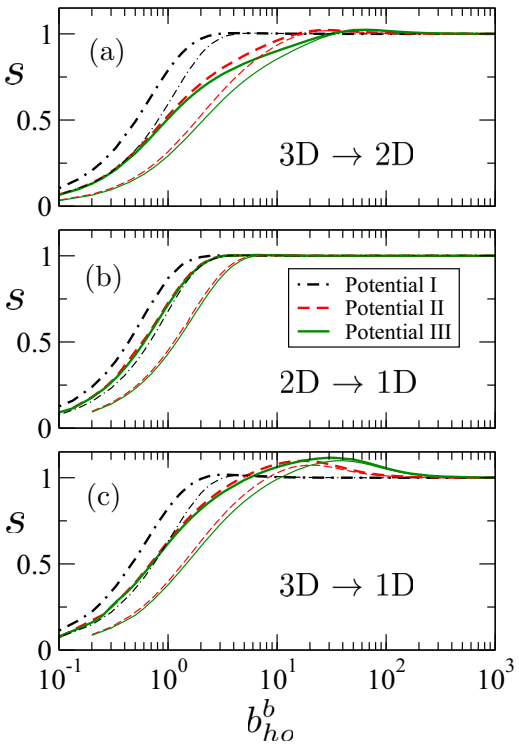

FIG. 6. The scale parameter s as a function of $b^b_{\rm ho}$ for the potentials in Table I and the three squeezing scenarios considered in this work.

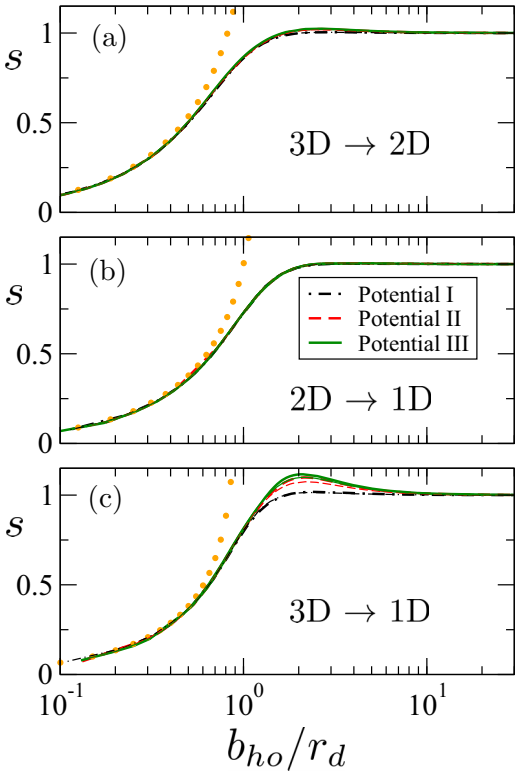

FIG. 7. The scale parameter s as a function of $b_{\rm ho}/r_d$, see Eq. (29), for the potentials in Table I and the three squeezing scenarios considered in this work. Except for panel (c) in the vicinity of $s = 1$, the curves corresponding to the Gaussian (thick curves) and Morse (thin curves) potentials are, to a large extent, indistinguishable. The circles show the analytical expression (47) valid for large squeezing.

than 1. This is very likely a consequence of using a constant scale parameter, or equivalently, that the perpendicular and squeezing directions are not completely decoupled for these short-range potentials.

The differences between the curves shown in Fig. 6 are related to the size of the two-body system in the initial dimension. In panels (a) and (c), potential III describes a two-body system in 3D clearly bigger than the other potentials (see Table I), and therefore the curve corresponding to this potential is the first one feeling the squeezing; i.e., it is the first one for which s deviates from 1 when the squeezing parameter, $b^b_{\rm ho}$ decreases. For the same reason the second potential feeling the squeezing is potential II, and for potential I the deviation from $s = 1$ starts for even smaller values of $b^b_{\rm ho}$. For the 2D → 1D case, Fig. 6(b), the curves corresponding to potentials II and III are very similar, since these two potentials describe systems with a very similar size in 2D (see Table I).

For the same reason there is a clear dependence on the potential shape. In general, given a squeezing parameter, the root-mean-square radius is clearly bigger with the Morse potential than in the Gaussian case, as seen for instance in Table I with the $r_{\rm 2D}$ and $r_{\rm 1D}$ values. This fact implies that, for a given $b^b_{\rm ho}$, the scale parameter in the case of using the Morse potential is clearly smaller than when the Gaussian potential is used.

A simple way to account for these size effects is to plot the scale parameter, s, as a function of $b_{\rm ho}/r_d$, where r_d is the root-mean-square radius of the system for dimension d as given in Eq. (29). This is shown in Fig. 7, where we can see that for all three potentials and the Gaussian and Morse shapes, the curves collapse into a single universal curve. The only discrepancy appears in panel (c) in the region where the squeezing begins to produce some effect, where the bump shown by potentials II and III is not observed in the case of potential I. This also happens, although to a much smaller extent, in the 3D → 2D case shown in panel (a). We also show in Fig. 7 (dots) the analytical expression given in Eq. (47), which gives the relation between s and $b_{\rm ho}/r_d$ in the case of large squeezing, i.e., in the case of small $b_{\rm ho}$ values. As we can see, the analytical expression can be used for values of $b_{\rm ho}/r_d \lesssim 0.5$.

It is also interesting to show the scale parameter, s, as a function of $u_{\rm rms}/r_d$, where $u_{\rm rms} = \langle u^2\rangle^{1/2}$, and u corresponds to z, y, or $r_\perp$ depending on what squeezing process we are dealing with, 3D → 2D, 2D → 1D, or 3D → 1D. Such relation should be governed by the expression given in Eq. (46). The result is shown in Fig. 8, where the scale parameter $[\times\sqrt{(d_i - d_f)/d_f}]$ is plotted as a function of $u_{\rm rms}/r_d$. As we can see, all the curves for all the squeezing cases are very similar to each other. The main difference appears in the low squeezing region. In fact, in the case of no squeezing the value of $u_{\rm rms}/r_d$ is different for each case, $1/\sqrt{3}$, $1/\sqrt{2}$, or $\sqrt{2/3}$, as indicated by the arrows in the figure. The dotted curve is the analytical form in Eq. (46), which for $u_{\rm rms}/r_d \lesssim 0.4$ reproduces quite well the computed curves.

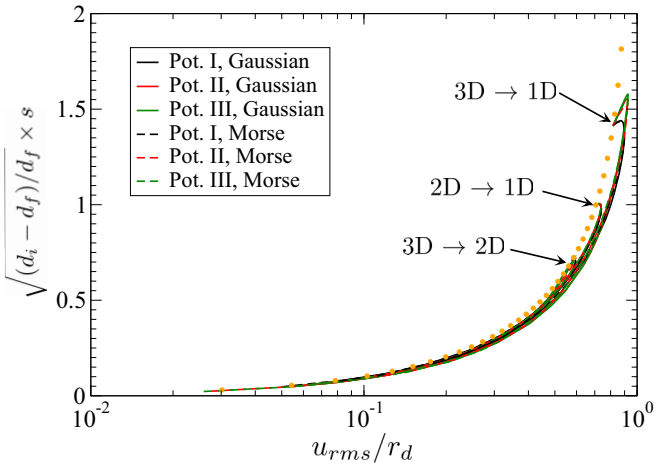

FIG. 8. The scale parameter s [$\times\sqrt{(d_i-d_f)/d_f}$] as a function of $u_{\rm rms}/r_d$ for the potentials in Table I, where $u=z$, $u=y$, and $u=r_\perp$ for 3D → 2D, 2D → 1D, and 3D → 1D, respectively. The circles show the analytical expression (46) valid for large squeezing.

Finally, it is clear from Figs. 7 and 8 that it is also possible to relate $b_{\rm ho}/r_d$ and $u_{\rm rms}/r_d$, simply by connecting the values of these two quantities corresponding to the same value of the scale parameter. For large squeezing, this relation should in fact be determined by Eq. (40). The result is shown in Fig. 9, where the factors multiplying $u_{\rm rms}/r_d$ and $b_{\rm ho}/r_d$ [$\sqrt{d_i/2}$ and $\sqrt{d_i/(d_i-d_f)}$] have been chosen in such a way that all the curves follow very much a rather universal curve. Only some of the curves show some discrepancy in the region of very small squeezing. In particular this is what happens with potentials II and III in the 3D → 1D case, which produce the bump that differs from the rest of the curves for $\sqrt{d_i/(d_i-d_f)}\langle r_\perp^2\rangle^{1/2}/r_d\approx 1$. This is the same deviation from the universal curve observed in Fig. 7(c) for these two potentials. This universal behavior is quite well reproduced using Eq. (40), which, as shown by the dotted line, follows

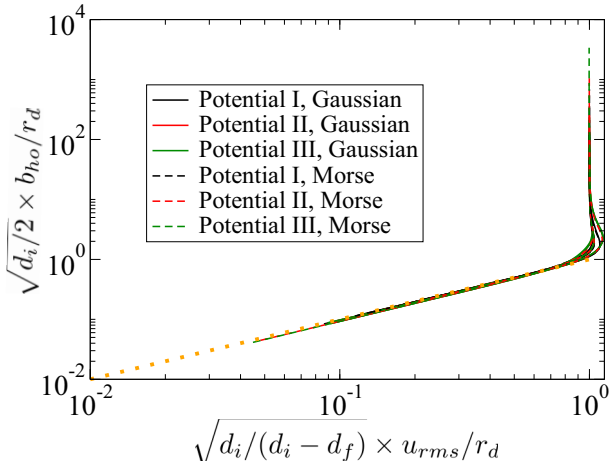

FIG. 9. Value of $b_{\rm ho}/r_d$ ($\times\sqrt{d_i/2}$) as a function of $u_{\rm rms}/r_d$ [$\times\sqrt{d_i/(d_i-d_f)}$] for the potentials in Table I, where $u=z$, $u=y$, and $u=r_\perp$ for 3D → 2D, 2D → 1D, and 3D → 1D, respectively. The dotted line is obtained from Eq. (40).

the computed curves almost up to the region where the discrepancy mentioned above shows up.

VII. UNIVERSAL RELATIONS

Some of the results shown in the previous section show what we could consider a universal behavior. The curves shown in Fig. 7 are very much independent of the scattering length of the potential, and of the shape of the potential. Furthermore, the curves shown in Fig. 8, and specially the ones in Fig. 9, can also be considered independent of the squeezing process.

One could then think that from these universal curves it should be possible to determine the dimension d that should be used to mimic the squeezing process produced by an external field with squeezing parameter $b_{\rm ho}$. This is however not so simple, since, for instance in Fig. 7, we relate s not just with $b_{\rm ho}$, but with $b_{\rm ho}/r_d$, and r_d is the root-mean-square radius in the d calculation, Eq. (29), where d must be the dimension associated with the squeezing parameter, $b_{\rm ho}$. In other words, use of the universal curves in Fig. 7 to obtain the s value corresponding to some squeezing parameter, $b_{\rm ho}$, requires previous knowledge of the relation between d and $b_{\rm ho}$. The same happens in Fig. 8, where $u_{\rm rms}$ is the root-mean-square radius in the squeezing direction, which can be computed only after knowing the scale parameter, obtained after maximization of Eqs. (37) or (38), which again requires previous knowledge of the value of $b_{\rm ho}$ associated with a given dimension. The same problem appears in Fig. 9.

However, Figs. 7 to 9 can be used to estimate the relation between d and $b_{\rm ho}$ in an indirect way. For instance, in Fig. 10(a) we show the universal curves shown in Fig. 8 for the 3D → 2D case. On top we plot for three different dimensions, $d=2.25$, $d=2.50$, and $d=2.75$, the curves (squares) showing $\langle z^2\rangle^{1/2}/r_d$ as a function of the scale parameter, s, for one of the potentials used in this work, in particular for the Morse potential II. The points where these curves cut the universal curve determine the specific values of s and $\langle z^2\rangle^{1/2}$ corresponding to each dimension [note that r_d is simply given by Eq. (29), and it does not depend on s]. Due to the numerical uncertainty in the universal curve, we have also considered the uncertainty (light-blue rectangles) in where the crossing is actually taking place. The results of the estimate for these three dimensions are given in Table II, where the second column shows the r_d value for each dimension, and the third and fourth columns give the estimated range obtained from Fig. 10(a) for $\langle z^2\rangle^{1/2}$ and s, respectively. Within parentheses we give the precise value obtained from the calculation. As one can see, the estimate is reasonably good.

Once the s value is known, we can use Fig. 7 (or Fig. 9), as shown in Fig. 10(b), to determine the values of $b_{\rm ho}$ that correspond to each of the dimensions considered. The results obtained are given in the last column of Table II, together with the computed values which are given within parentheses.

In any case, it is obvious that a direct connection between d and $b_{\rm ho}$ is highly desirable. In fact, as shown in Fig. 5, at least the curves corresponding to potentials II and III (the ones having a large scattering length) show very much the same behavior for a given potential shape, but even if we consider

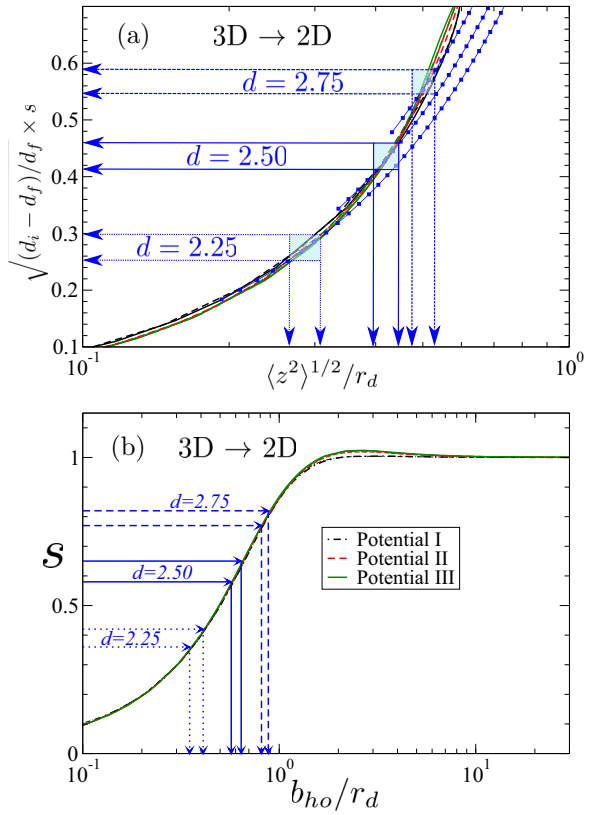

FIG. 10. (a) The same as in Fig. 8 for the 3D → 2D case, where we show (squares) the computed values of $\langle z^2 \rangle^{1/2}/r_d$ as a function of the scale parameter s for three different dimensions, $d = 2.25$, 2.50, and 2.75. (b) The same as in Fig. 7(b) where the arrows indicate the values of $b_{\rm ho}/r_d$ corresponding to the scale parameter s where the squared lines in the upper part cut the universal curve.

the results with the Gaussian and Morse potentials, the curves are not far from being universal.

An attempt of making the curves in Fig. 5 fully universal was introduced in [16], which can be generalized to a general d_iD → d_fD squeezing process as

$$\tilde{b}_{\rm ho} = b_{\rm ho}\left(1 + \sqrt{\frac{b_{\rm ho}^2 + r_{d_f{\rm D}}^2}{a_{d_i{\rm D}}^2 + r_{d_f{\rm D}}^2}}\right). \tag{48}$$

The result of this transformation is shown in Fig. 11. As we can see, the effect of the scattering length being comparable to the range of the potential is corrected to a large extent, and

TABLE II. Estimate of $\langle z^2 \rangle^{1/2}$, the scale parameter s, and the squeezing parameter $b_{\rm ho}^b$ for the Morse potential II, obtained from the universal curves as shown in Fig. 10 for the dimensions $d = 2.25$, $d = 2.50$, and $d = 2.75$. Their corresponding r_d values are given in the second column of the table. All the lengths are given in units of the range of the interaction. The numbers within parentheses are the values obtained from the calculations.

d	r_d	$\langle z^2 \rangle^{1/2}$	s	$b_{\rm ho}^b$
2.25	3.33	0.89–1.05 (0.96)	0.36–0.42 (0.39)	1.17–1.37 (1.30)
2.50	4.24	1.69–1.90 (1.77)	0.58–0.65 (0.61)	2.43–2.69 (2.57)
2.75	6.00	2.88–3.15 (3.11)	0.77–0.82 (0.81)	4.92–5.40 (5.38)

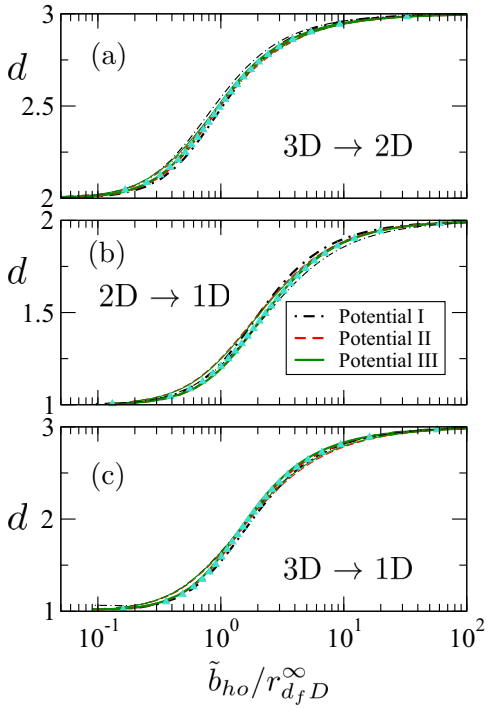

FIG. 11. The same as Fig. 5, but after the transformation defined in Eq. (48).

all the curves follow a rather universal curve for each of the d_iD → d_fD squeezing processes.

In Fig. 11 we also show an analytical fit (triangles) that reproduces very well the universal curve for each of the squeezing scenarios. Since the curve is model independent, the special form of the fitting function is unimportant provided it gives a sufficiently accurate connection between $\tilde{b}_{\rm ho}$ and d. We have different options but one possibility is

$$\frac{\tilde{b}_{\rm ho}}{r^{\infty}_{d_f{\rm D}}} = c_1\left(\frac{d - d_f}{d_i - d}\right)^{d_i/3} + c_2 \tan\left[\left(\frac{d - d_f}{d_i - d_f}\right)^{c_3}\frac{\pi}{2}\right], \tag{49}$$

which is a combination of two functions, each of them being equal to zero at $d = d_f$, and to ∞ at $d = d_i$, and whose relative weight is used to fit the curves between these two limits. The computed fitting constants for each of the three squeezing processes are given in Table III.

It is important to mention that, in principle, instead of the two-body energy, as shown in Figs. 3 and 4, one could have used a different observable in order to determine the connection between d and the squeezing parameter, $b_{\rm ho}$. We have checked that when the root-mean-square radii are used, the same universal relation as the one shown in Fig. 11 is

TABLE III. Parameters used in the numerical fit given in Eq. (49) giving rise to the curves indicated by the triangles in Fig. 11.

	c_1	c_2	c_3
3D → 2D	−0.28	0.78	0.62
2D → 1D	1.34	0.24	0.25
3D → 1D	−0.41	1.12	0.54

obtained. The main practical problem in this case is that, in general, the convergence of the computed radii when the external squeezing is considered is clearly slower than the convergence of the energy. Even larger values of the two-body relative angular momenta are needed in the expansion (3), which actually is a source of numerical inaccuracies, especially for large squeezing scenarios.

VIII. SUMMARY AND CONCLUSIONS

We investigate in detail how a dimension-dependent centrifugal barrier can be the substitute for an external one-body potential. We choose the ground state of a simple two-body system with Gaussian and Morse short-range interactions. The dimension parameter is integer in the initial formulations, which in this report are analytically continued to allow noninteger dimensional values. The external potential is chosen as both the experimentally and theoretically practical harmonic oscillator which in the present context necessarily must be anisotropic or deformed. A well defined unique transformation between the parameters of the two methods then makes each of them complete with precise predictions of results from the other method. The simpler centrifugal barrier computations are then sufficient to provide observables found with an external potential.

The overall idea is then to start with an ordinary integer dimension of 3, 2, or perhaps 1, and apply an increasingly confining external potential in one or more coordinates. This is equivalent to increasing frequency or decreasing oscillator length in the corresponding directions while other coordinates are left untouched. The process leads from one integer dimension to another lower one. The results are compared with calculations without external potential but with a dimension-dependent centrifugal barrier where the same initial and final configurations are assumed and mathematically correct. The aim is to establish a desired unique relation between the dimension parameter and the oscillator squeezing length.

We first describe in detail how the harmonic oscillator confinement is implemented in the investigated transitions, $3D \to 2D$, $2D \to 1D$, and $3D \to 1D$. The center-of-mass and relative coordinates are separated, and the conserved quantum numbers for the ground states are specified. Second, we discuss properties of the calculations for the noninteger dimension formulation. A crucial part is here how to interpret the resulting wave function in terms of the deformed solution with an external potential. We express how a scaling of the squeezed coordinate(s) on the "spherically symmetric" noninteger dimensional wave function resembles the solution with a deformed external potential.

The final results are the unique transformation between the two methods. This is for each dimensional transition explicitly given as a one-to-one correspondence between oscillator squeezing length and wave-function scaling and dimension parameters. To be useful it must be independent of the choice of the short-range interaction. This can be achieved if the transformation relation is formulated in terms of either universal quantities or, sufficient for our purpose, quantities obtainable entirely within the simple dimension calculation. Both of these cases qualify to be denoted universal relations provided the results only depend on these quantities, being independent of dimensional transition and short-range interaction.

In summary, we have first established universal relations. Second, we provided the universal interpretation in terms of analytic fitted functions, which relate oscillator squeezing length with dimension and wave-function scaling parameters. These fitted functions allow predictions from noninteger dimension calculations of observables in trap experiments with external potentials. For two-body systems the one-to-one correspondence does not provide enormous savings. However, the idea and the insight obtained through these universal relations present a new and hopefully useful concept.

In perspective, the present elaborate report on two-body physics of noninteger dimensions constitutes the first step in a larger program. The immediate next investigations are two-body systems without bound states in three dimensions, then three particles, first with identical bosons and then with nonidentical particles. These extensions are each rather big steps presenting their own difficulties. In conclusion, we have worked on a simple system to exhibit new principles, but the door is now open to more complicated and more interesting systems.

ACKNOWLEDGMENT

This work was supported by funds provided by the Ministry of Science, Innovation, and Universities (Spain) under Contract No. PGC2018-093636-B-I00.

APPENDIX: THE SCALE PARAMETER AND EXPECTATION VALUES IN THE SQUEEZING DIRECTION

1. 3D → 2D

In this case the radial coordinate, r, is redefined as given in Eq. (30):

$$r \to \tilde{r} \equiv \sqrt{x^2 + y^2 + (z/s)^2} \equiv \sqrt{r_\perp^2 + (z/s)^2}. \tag{A1}$$

The normalization of the wave function (23) requires calculation of

$$\mathcal{N}_s = \int r_\perp dr_\perp dz d\varphi |\Psi_d(\tilde{r})|^2, \tag{A2}$$

which, after defining $u = z/s$, can be rewritten as

$$\mathcal{N}_s = s \int r_\perp dr_\perp du d\varphi |\Psi_d(\tilde{r})|^2 = s\mathcal{I}_0, \tag{A3}$$

where $\tilde{r}^2 = r_\perp^2 + u^2$ and the integral, $\mathcal{I}_0$, is independent of the scale parameter. Note that for $d = 3$, since $\Psi_{d=3}$ is already in the 3D space we then trivially have that $\mathcal{N}_{s=1} = 1$.

Therefore, the wave function, $\tilde{\Psi}_d = \Psi_d/\sqrt{\mathcal{N}_s}$, is normalized to 1 in the ordinary three-dimensional space. After this normalization we can now compute the expectation value,

$\langle z^2\rangle_s$, which given by

$$\langle z^2\rangle_s = \int z^2 r_\perp dr_\perp dz d\varphi |\tilde{\Psi}_d(\tilde{r})|^2, \tag{A4}$$

which, again under the transformation, $u = z/s$, takes the form

$$\langle z^2\rangle_s = \frac{s^3}{\mathcal{N}_s}\int u^2 r_\perp dr_\perp du d\varphi |\Psi_d(\tilde{r})|^2 = \frac{s^3}{\mathcal{N}_s}\mathcal{I}_2, \tag{A5}$$

where $\mathcal{I}_2$ is independent of s.

Making now use of Eq. (A3) we get

$$\langle z^2\rangle_s = s^2\frac{\mathcal{I}_2}{\mathcal{I}_0}, \tag{A6}$$

from which we get the final expression for the scale parameter:

$$s = \left(\frac{\langle z^2\rangle_s}{\langle z^2\rangle_{s=1}}\right)^{1/2}. \tag{A7}$$

2. 3D → 1D

In this case the radial coordinate, r, is redefined as given in Eq. (31):

$$r \to \tilde{r} \equiv \sqrt{(x^2+y^2)/s^2 + z^2} \equiv \sqrt{(r_\perp/s)^2 + z^2}. \tag{A8}$$

We then proceed exactly as in the 3D → 2D case, but using the transformation $u = r_\perp/s$. In this way the normalization constant (A2) reads now

$$\mathcal{N}_s = s^2\int u du dz d\varphi |\Psi_d(\tilde{r})|^2 = s^2\mathcal{I}_0. \tag{A9}$$

In the same way, under the same transformation, the expectation value

$$\langle r_\perp^2\rangle_s = \int r_\perp^3 dr_\perp dz d\varphi |\tilde{\Psi}_d(\tilde{r})|^2 \tag{A10}$$

can be rewritten as

$$\langle r_\perp^2\rangle_s = \frac{s^4}{\mathcal{N}_s}\int u^3 du dz d\varphi |\Psi_d(\tilde{r})|^2 = \frac{s^4}{\mathcal{N}_s}\mathcal{I}_2, \tag{A11}$$

which again, by use of Eq. (A9), leads to

$$s = \left(\frac{\langle r_\perp^2\rangle_s}{\langle r_\perp^2\rangle_{s=1}}\right)^{1/2}. \tag{A12}$$

3. 2D → 1D

In this case the radial coordinate, r, is redefined as given in Eq. (31),

$$r \to \tilde{r} \equiv \sqrt{x^2 + (y/s)^2}, \tag{A13}$$

and the normalization constant is given by

$$\mathcal{N}_s = \int dx dy |\Psi_d(\tilde{r})|^2 = s\int dx du |\Psi_d(\tilde{r})|^2 = s\mathcal{I}_0, \tag{A14}$$

where now $u = y/s$.

The expectation value, $\langle y^2\rangle_s$, is now

$$\langle y^2\rangle_s = \int y^2 dx dy |\tilde{\Psi}_d(\tilde{r})|^2 = \frac{s^3}{\mathcal{N}_s}\int u^2 dx du |\Psi_d(\tilde{r})|^2 = s^2\frac{\mathcal{I}_2}{\mathcal{I}_0}. \tag{A15}$$

As before, since $\mathcal{I}_0$ and $\mathcal{I}_2$ are s-independent, we then get the analogous result:

$$s = \left(\frac{\langle y^2\rangle_s}{\langle y^2\rangle_{s=1}}\right)^{1/2}. \tag{A16}$$

[1] E. Nielsen, D. V. Fedorov, A. S. Jensen, and E. Garrido, Phys. Rep. **347**, 373 (2001).
[2] B. Simon, Ann. Phys. **97**, 279 (1976).
[3] V. Efimov, Phys. Lett. B **33**, 563 (1970).
[4] L. W. Bruch and J. A. Tjon, Phys. Rev. A **19**, 425 (1979).
[5] T. K. Lim and B. Shimer, Z. Phys. A **297**, 185 (1980).
[6] D. S. Petrov and G. V. Shlyapnikov, Phys. Rev. A **64**, 012706 (2001).
[7] J. H. Sandoval, F. F. Bellotti, M. T. Yamashita, T. Frederico, D. V. Fedorov, A. S. Jensen, and N. T. Zinner, J. Phys. B **51**, 065004 (2018).
[8] D. S. Rosa, T. Frederico, G. Krein, and M. T. Yamashita, Phys. Rev. A **97**, 050701(R) (2018).
[9] M. T. Yamashita, F. F. Bellotti, T. Frederico, D. V. Fedorov, A. S. Jensen, and N. T. Zinner, J. Phys. B **48**, 025302 (2015).
[10] S. R. Beane and M. Jafry, J. Phys. B **52**, 035001 (2019).
[11] S. Lammers, I. Boettcher, and C. Wetterich, Phys. Rev. A **93**, 063631 (2016).
[12] D. J. Doren and D. R. Herschbach, Phys. Rev. A **34**, 2654 (1986).
[13] A. González, Few-Body Syst. **10**, 43 (1991).
[14] M. E. Peskin and D. V. Schroeder, *An Introduction to Quantum Field Theory* (Avalon Publishing, New York, 1995).
[15] M. Valiente, N. T. Zinner, and K. Mølmer, Phys. Rev. A **86**, 043616 (2012).
[16] E. Garrido, A. S. Jensen, and R. Álvarez-Rodríguez, Phys. Lett. A **383**, 2021 (2019).
[17] L. D. Landau and E. M. Lifshitz, in *Quantum Mechanics: Non-Relativistic Theory* (Pergamon Press, Oxford, UK, 1977), p. 114.
[18] S. I. Hayek, in *Advanced Mathematical Methods in Science and Engineering* (Marcel Dekker Inc., New York, 2001), p. 645.